Appendix C

Numerical Simulations

C.1 PN Junctions

In order to verify the validity of the numerical solutions and simulations used in the analysis of the detector PIN photodiodes, a numerical simulation of a simple one-dimensional PN junction has been conducted. The methodology follows closely that of Kurata [57] and MacCormack [126]. The results of these simulations match well with the analytical solution based upon the full depletion approximation as well as other simulations. A brief review of the techniques used will be given in this section.

C.2 Basic Semiconductor Physics

The crucial quantities in semiconductor analysis are the charge density, ρ, electric field, $\mathbf{E}$, electric potential, ϕ, the number of electrons in the conduction band, n_c (cm^{-3}), and the number of holes in the valence band p_v (cm^{-3}). As noted in Ashcroft and Mermin [127], conduction is entirely due to electrons in conduction band levels or holes in valence band levels. In order to describe the behavior of these quantities in a semiconductor with a dielectric constant of ϵ, we must apply the basic governing equations: Gauss's law,

$$\nabla \cdot \mathbf{E} = \frac{\rho}{\epsilon}, \tag{C.1}$$

Poisson's equation,

$$\nabla^2 \phi = -\frac{\rho}{\epsilon}, \tag{C.2}$$

and the continuity equations,

$$\frac{\partial n}{\partial t} = G_n - U_n + \frac{1}{q}\nabla \cdot \mathbf{J}_n, \tag{C.3}$$

$$\frac{\partial p}{\partial t} = G_p - U_p + \frac{1}{q}\nabla \cdot \mathbf{J}_p. \tag{C.4}$$

G_n and G_p are the electron and hole generation rate ($\mathrm{cm}^{-3}/\mathrm{s}$), respectively, and U_n and U_p are the corresponding recombination rates. $\mathbf{J}_n$ and $\mathbf{J}_p$ are the electron and hole current densities, respectively,

$$\mathbf{J}_p = q\mu_p p\mathbf{E} - qD_p\nabla p \tag{C.5}$$

$$\mathbf{J}_n = q\mu_n n\mathbf{E} + qD_n\nabla n. \tag{C.6}$$

μ_p and μ_n are the mobilities and D_p and D_n are the diffusion constants for holes and electrons, respectively. Each can be determined from the other via the Einstein relations $D_{p,n} = (kT/q)\mu_{p,n}$. In principle, the mobilities might be dependent on the electric field or position in the material. Here we will neglect any such dependencies. The charge density in the material has contributions from n_c and p_v along with the ionized donor impurity atoms, N_d^+, and ionized acceptor impurity atoms, N_a^-:

$$\rho = q(p_v - n_c + N_d^+ - N_a^-) \tag{C.7}$$

With these equations and proper expressions for G and R, we can appropriately describe the dynamics of the system. We shall neglect magnetic fields and external electric fields.

C.3 Numerical Methods: Finite Volume Scheme

To calculate the fields and concentrations numerically, we use a finite-difference scheme and a simple one-dimensional model represented by the diagram in Figure C.1 The concentrations and potentials are defined at grid points i and the electric field and current densities at grid points $i \pm 1/2$. The material extends from $x_0 = 0$ μm to $x_I = 2$ μm. In this simple case, a uniform grid is used, so $\Delta x_i = \Delta x_{i\pm1/2}$ is a constant. However, for other simulations where I is sufficiently large (i.e. for the 100 μm thick PIN diodes) a non-uniform grid is used. In these cases, the grid spacing is made very fine in regions where the physical quantities are expected to change rapidly and coarse in areas where they are expected to vary slowly. The separations between adjacent points are then given by the relation

$$\Delta x_{i\pm1/2} = (\Delta x_i + \Delta x_{i\pm1})/2 \tag{C.8}$$

The extension to 2 dimensions is straightforward. It simply involves placing another grid in the y direction and overlaying these two grids to form a mesh. In a similar fashion, we discretize time at points t_k, with $k = 0, 1, 2, ...$, and use a constant separation

$$\Delta t = t_{k+1} - t_k. \tag{C.9}$$

This allows approximations of time-derivatives.

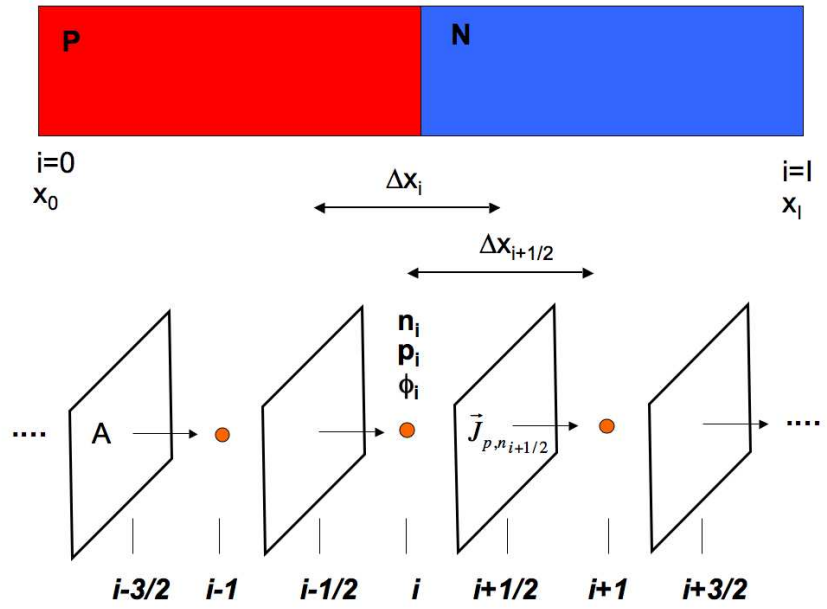

Figure C.1: Diagram showing configuration for the PN junction. The grid is staggered so that $\mathbf{E}$ and $\mathbf{J_{p/n}}$ are defined at half-integer values of $i \pm 1/2$ while the charge density and potential are defined at integer values i. The distance between x_i and x_{i+1} is $\Delta x_{i+1/2}$ and the distance between $x_{i-1/2}$ and $x_{i+1/2}$ is Δx_i. The surface enclosing the charge has area A on each side.

In the discrete approximation over the 1-d grid, Equations C.2-C.4 take the form,

$$\frac{p_i^{k+1} - p_i^k}{\Delta t} = -(1-\alpha)\left(\frac{J_{p,i+1/2}^k - J_{p,i-1/2}^k}{q\Delta x_i} - G_{p,i}^k + U_{p,i}^k\right) - \alpha\left(\frac{J_{p,i+1/2}^{k+1} - J_{p,i-1/2}^{k+1}}{q\Delta x_i} - G_{p,i}^{k+1} + U_{p,i}^{k+1}\right) \tag{C.10}$$

$$\frac{n_i^{k+1} - n_i^k}{\Delta t} = (1-\alpha)\left(\frac{J_{n,i+1/2}^k - J_{n,i-1/2}^k}{q\Delta x_i} - G_{n,i}^k - U_{n,i}^k\right) + \alpha\left(\frac{J_{n,i+1/2}^{k+1} - J_{n,i-1/2}^{k+1}}{q\Delta x_i} - G_{n,i}^{k+1} - U_{n,i}^{k+1}\right) \tag{C.11}$$

$$\frac{\phi_{i+1}^k - 2\phi_i^k + \phi_{i-1}^k}{\Delta x_i^2} = \frac{-q(p_i^k - n_i^k + N_{d,i}^+ - N_{a,i}^-)}{\epsilon} = \frac{-\rho_i}{\epsilon} \tag{C.12}$$

If we set $\alpha = 0$, we will have an *explicit* set of equations that can be solved with a very easy to code

algorithm for a steady state solution. At each time step k, the potential ϕ^k is solved for based upon the charge density at k. This potential is then used to calculate the new charge density at $k+1$. However, this method converges extremely slowly, taking anywhere from hours to days depending on the initial conditions used. This is because the method is unstable and requires a very small value for Δt to advance towards the solution.

If, on the other hand, we set $\alpha = 1/2$ or $\alpha = 1$, we will be using a *semi-implicit* or *implicit* method, respectively. The case of $\alpha = 1/2$ is often refereed to as the Crank-Nicolson method [126]. These methods converge much faster than the explicit method due to their increased stability. However, the algorithms are much more difficult to implement numerically due to the fact that we must solve the three coupled equations simultaneously because we do not know what values the quantities have at $k+1$. Not to mention, two of them are nonlinear.

To overcome the difficulty of nonlinearity, we must first linearize the equations. The current densities as well as the generation and recombination rates all require linearization. As an example, we first write the hole current density at time t_{k+1} as

$$J_{p,i+1/2}^{k+1} = J_{p,i+1/2}^{k} + \delta J_{p,i+1/2}. \tag{C.13}$$

If we neglect second-order terms and higher, the Taylor expansion of the change in $J_{p,i}$ from time-step k to $k+1$ can be expressed as

$$\delta J_{p,i+1/2} = \frac{\partial J_{p,i+1/2}}{\partial p_i}\delta p_i + \frac{\partial J_{p,i+1/2}}{\partial p_{i+1}}\delta p_{i+1} + \frac{\partial J_{p,i+1/2}}{\partial \phi_i}\delta \phi_i + \frac{\partial J_{p,i+1/2}}{\partial \phi_{i+1}}\delta \phi_{i+1}. \tag{C.14}$$

Similar expressions can be written for G_p, U_p, J_n, G_n, and U_n. The usefulness of the Taylor expansion becomes apparent after a few more steps and substitutions. We first write Equations C.10- C.12 as:

$$\frac{1}{\Delta t}\delta p + \alpha\frac{D_i}{q}\delta J_{p,i} + \alpha\delta G_{p,i} - \alpha\delta U_{p,i} = -\frac{D_i}{q}J_{p,i}^k + G_{p,i}^k - U_{p,i}^k \tag{C.15}$$

$$\frac{1}{\Delta t}\delta n - \alpha\frac{D_i}{q}\delta J_{n,i} + \alpha\delta G_{n,i} - \alpha\delta U_{n,i} = \frac{D_i}{q}J_{n,i}^k + G_{n,i}^k - U_{n,i}^k \tag{C.16}$$

$$D_i^2\delta\phi_i = -\frac{\rho_i^k}{\epsilon} + D_i^2\phi_i^k \tag{C.17}$$

where D_i and D_i^2 are second-order centered difference operators defined such that

$$D_i(f) = \frac{f_{i+1/2} - f_{i-1/2}}{\Delta x_i} \tag{C.18}$$

$$D_i^2(f) = \frac{f_{i+1}}{\Delta x_{i+1}\Delta x_{i+1/2}} - \frac{f_i}{\Delta x_i\Delta x_{i+1/2}} - \frac{f_i}{\Delta x_i\Delta x_{i-1/2}} + \frac{f_{i-1}}{\Delta x_{i-1}\Delta x_{i-1/2}}. \tag{C.19}$$

Then we introduce the vectors

$$\Theta = \begin{pmatrix} p \\ n \\ \phi \end{pmatrix} \qquad \delta\Theta = \begin{pmatrix} \delta p \\ \delta n \\ \delta\phi \end{pmatrix},$$

With these vectors and the introduction of several new matrices, the three coupled equations can be written as one matrix equation:

$$\begin{aligned} \alpha\left[\frac{\tilde{J}_{i-1/2,i-1}}{q} + \tilde{G}_{i,i-1} + \tilde{U}_{i,i-1}\right]\delta\Theta_{i-1} + \\ \left[T_i + \alpha\left(\frac{\tilde{J}_{i-1/2,i} - \tilde{J}_{i+1/2,i}}{q} + \tilde{G}_{i,i} + \tilde{U}_{i,i}\right)\right]\delta\Theta_i + \\ \alpha\left[\frac{\tilde{J}_{i+1/2,i+1}}{q} + \tilde{G}_{i,i+1} + \tilde{U}_{i,i+1}\right]\delta\Theta_{i+1} = F_i \end{aligned} \tag{C.20}$$

The notation is quite cumbersome and care must be taken with the double indices to ensure the derivatives are being approximated correctly. $\tilde{J_{i+1/2,i}}$, $\tilde{G_{i,i}}$, $\tilde{U_{i,i}}$, etc., are the 3×3 Jacobian of their respective variables and coordinates that handle the linearization. As an example,

$$\tilde{G}_{i,i+1} = \begin{pmatrix} \frac{\partial G_{p,i}}{\partial p_{i+1}} & 0 & \frac{\partial G_{p,i}}{\partial \phi_{i+1}} \\ 0 & \frac{\partial G_{n,i}}{\partial n_{i+1}} & \frac{\partial G_{n,i}}{\partial \phi_{i+1}} \\ 0 & 0 & 0 \end{pmatrix}, \quad \tilde{U}_{i,i+1} = \begin{pmatrix} \frac{\partial U_{p,i}}{\partial p_{i+1}} & 0 & \frac{\partial U_{p,i}}{\partial \phi_{i+1}} \\ 0 & \frac{\partial U_{n,i}}{\partial n_{i+1}} & \frac{\partial U_{n,i}}{\partial \phi_{i+1}} \\ 0 & 0 & 0 \end{pmatrix}$$

$$\tilde{J}_{i+1/2,i} = \begin{pmatrix} \frac{\partial J_{p,i+1/2}}{\partial p_i} & 0 & \frac{\partial J_{p,i+1/2}}{\partial \phi_i} \\ 0 & \frac{\partial J_{n,i+1/2}}{\partial n_i} & \frac{\partial J_{n,i+1/2}}{\partial \phi_i} \\ 0 & 0 & 0 \end{pmatrix}$$

and T_i and F_i are given by:

$$T_i = \begin{pmatrix} \frac{1}{\Delta t} & 0 & 0 \\ 0 & \frac{1}{\Delta t} & 0 \\ 0 & 0 & D_i^2 \end{pmatrix}, \quad F_i = \begin{pmatrix} -\frac{D_i}{q}J_{p,i}^k + G_{p,i}^k - U_{p,i}^k \\ \frac{D_i}{q}J_{n,i}^k + G_{n,i}^k - U_{n,i}^k \\ \frac{\rho_i^k}{\epsilon} + D_i^2\phi_i^k \end{pmatrix}$$

All of the quantities on the right-hand side of Equation C.20 are known at time-step t_k (at t_0 we supply a suitable initial guess) and the left-hand side represents a block tri-diagonal matrix multiplying the array of unknown column vectors $\delta\Theta$. To solve for $\delta\Theta$ we must invert this matrix with techniques such as the ones in [126] and [57]. In the case where a steady-state solution is sought, we solve for $\delta\Theta$ at each time t_k until $\delta\Theta \sim 0$.

The elements with values at $i = 0$ and $i = I$ must be handled separately, first, because they do

not have surrounding points at $i = -1$ and $i = I + 1$, and second, because they physically represent the supplied boundary conditions. For an ideal PN junction, the requirement is that the space charge density and electric field at the boundaries vanish and that the built-in electric potential takes its thermal equilibrium values. The first of these conditions, along with the law of mass-action that relates the electron and hole concentrations to the intrinsic concentration, n_{int}, yields

$$\begin{aligned} p_0 &= -\frac{N_{d,0} - N_{a,0}}{2}\left\{1 + \left[1 + \left(\frac{2n_{int}}{N_{d,0} - N_{a,0}}\right)^2\right]^{1/2}\right\} \quad , \quad n_0 = \frac{n_{int}^2}{p_0} \\ n_I &= \frac{N_{d,I} - N_{a,I}}{2}\left\{1 + \left[1 + \left(\frac{2n_{int}}{N_{d,I} - N_{a,I}}\right)^2\right]^{1/2}\right\} \quad , \quad p_I = \frac{n_{int}^2}{n_I} \end{aligned} \tag{C.21}$$

while the second results in

$$\phi_0 = -\frac{kT}{q}\ln\left[\frac{p_0}{n_{int}}\right] \qquad , \qquad \phi_I = V_{bias} + \frac{kT}{q}\ln\left[\frac{n_I}{n_{int}}\right] \tag{C.22}$$

where V_{bias} is the applied bias voltage. In the case of the PIN diodes, this will take the value of the substrate voltage, V_{SUB}, and will be enforced on the n^+ side of the junction.

The last point to consider before the equations are solved is a very subtle one; one that often causes headaches when implementing numerical methods. As shown by Scharfetter and Gummel [128], instability of the solution occurs when $|\phi_{i+1} - \phi_i| > 2kT/q$. One way to get around this is to make the space between grid points sufficiently small. The price one pays for this is increased computation time. An alternative way is to assume the current densities and electric field are constant in between grid points and instead to solve a differential equation to approximate $J_{p,n}$ at these location. The technique is referred to as Scharfetter-Gummel discretization and it results in the following expressions for the current densities:

$$\begin{aligned} J_{p,i+1/2} &= -\frac{q\mu_p}{\Delta x_{i+1/2}}\left[\left(\frac{\phi_i - \phi_{i+1}}{1 - e^{-q(\phi_i - \phi_{i+1})/kT}}\right)p_i + \left(\frac{\phi_i - \phi_{i+1}}{1 - e^{q(\phi_i - \phi_{i+1})/kT}}\right)p_{i+1}\right] \\ J_{n,i+1/2} &= -\frac{q\mu_n}{\Delta x_{i+1/2}}\left[\left(\frac{\phi_i - \phi_{i+1}}{1 - e^{q(\phi_i - \phi_{i+1})/kT}}\right)n_i + \left(\frac{\phi_i - \phi_{i+1}}{1 - e^{-q(\phi_i - \phi_{i+1})/kT}}\right)n_{i+1}\right] \end{aligned} \tag{C.23}$$

It is from these expressions that the partial derivatives in the Jacobians $\tilde{J}$ are calculated. For the exact matrix elements, the reader is referred to Kurata [57].

C.4 Results for Abrupt PN Junction

The actual implementation of this numerical method is carried out via a python script that makes use of the numpy and scipy libraries. As a test, we consider the abrupt junction shown in Figure

C.1 in which the P and N regions are both 1 μm in length. The doping densities are set such that $N_d = 0$ cm^{-3} and $N_a = 10^{18}$ cm^{-3} on the P side and $N_d = 10^{19}$ cm^{-3} and $N_a = 0$ cm^{-3} on the N side. The value of the intrinsic carrier density is $n_{int} = 10^{10}$ cm^{-3}. An implicit method ($\alpha = 1$) is used and 70 time steps of $\Delta t = 10^{-12}$ s are taken to reach the steady state solution. Larger values of Δt result in instabilities that cause the solution to diverge.

The results of a simulation with V_{bias} =0 V are shown in Figure C.2. The dashed lines on the plots indicate the depletion region boundaries obtained from the full depletion approximation. $x_p = 34.6$ nm is the distance the depletion region extends into the p material and $x_n = 3.46$ nm is the distance it extends into the n material. In the full depletion approximation, the changes in space charge densities occur as step discontinuities at the boundaries of the depletion region. The numerical solution does not have this simplification built in and shows that these transitions are indeed smooth as one would expect. They do not begin or end at the calculated boundaries, but rather are centered around them. The potential and number densities also vary in agreement with the analytical calculation, but show some variation outside the depletion region boundaries. The case of $V_{bias} = 1.2$ V is shown in Figure C.3. As expected, the size of the depletion region is increased. It reaches further into the less heavily doped p region then it does into the n region.

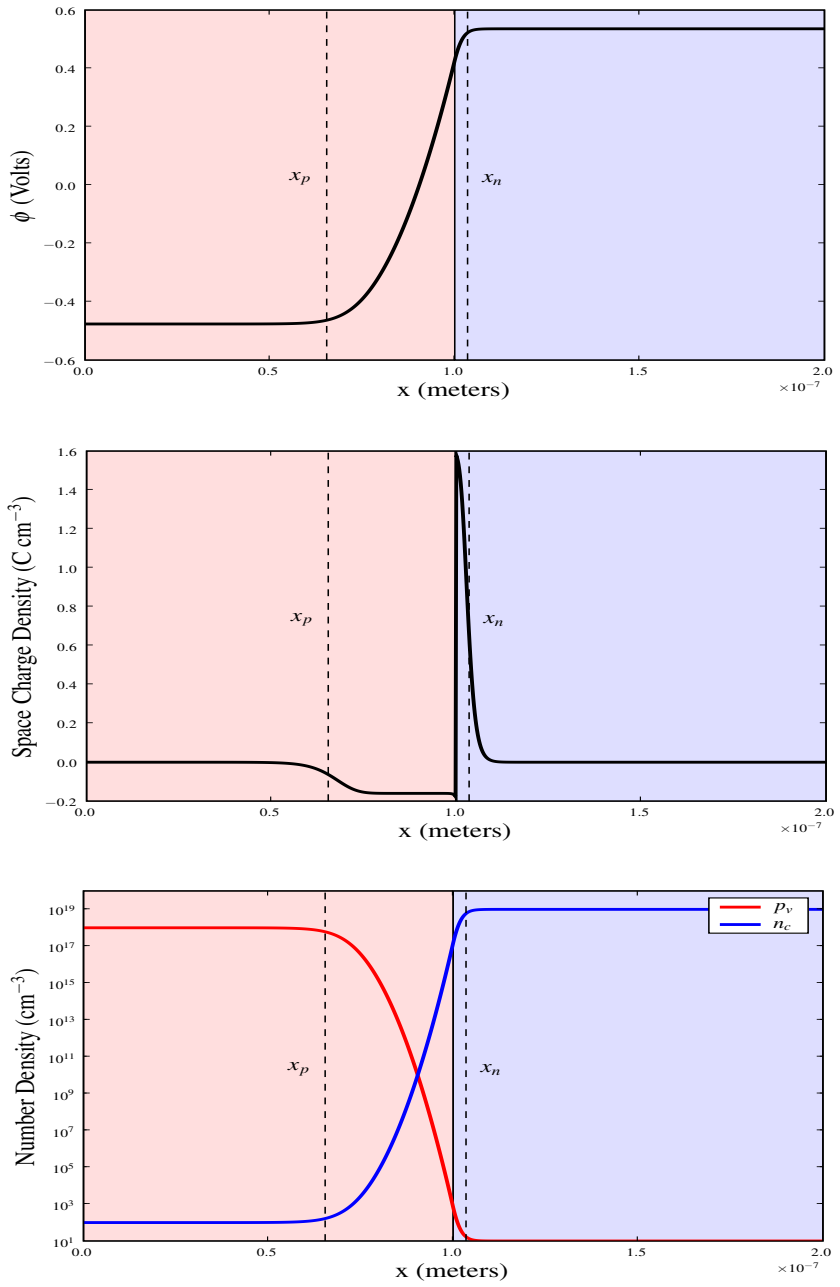

Figure C.2: Potential (ϕ), charge density, and number density of holes and electrons for the numerical simulation of an abrupt PN junction with no bias voltage applied. The depletion region boundaries x_p and x_n obtained from the analytical calculation are shown on the plots.

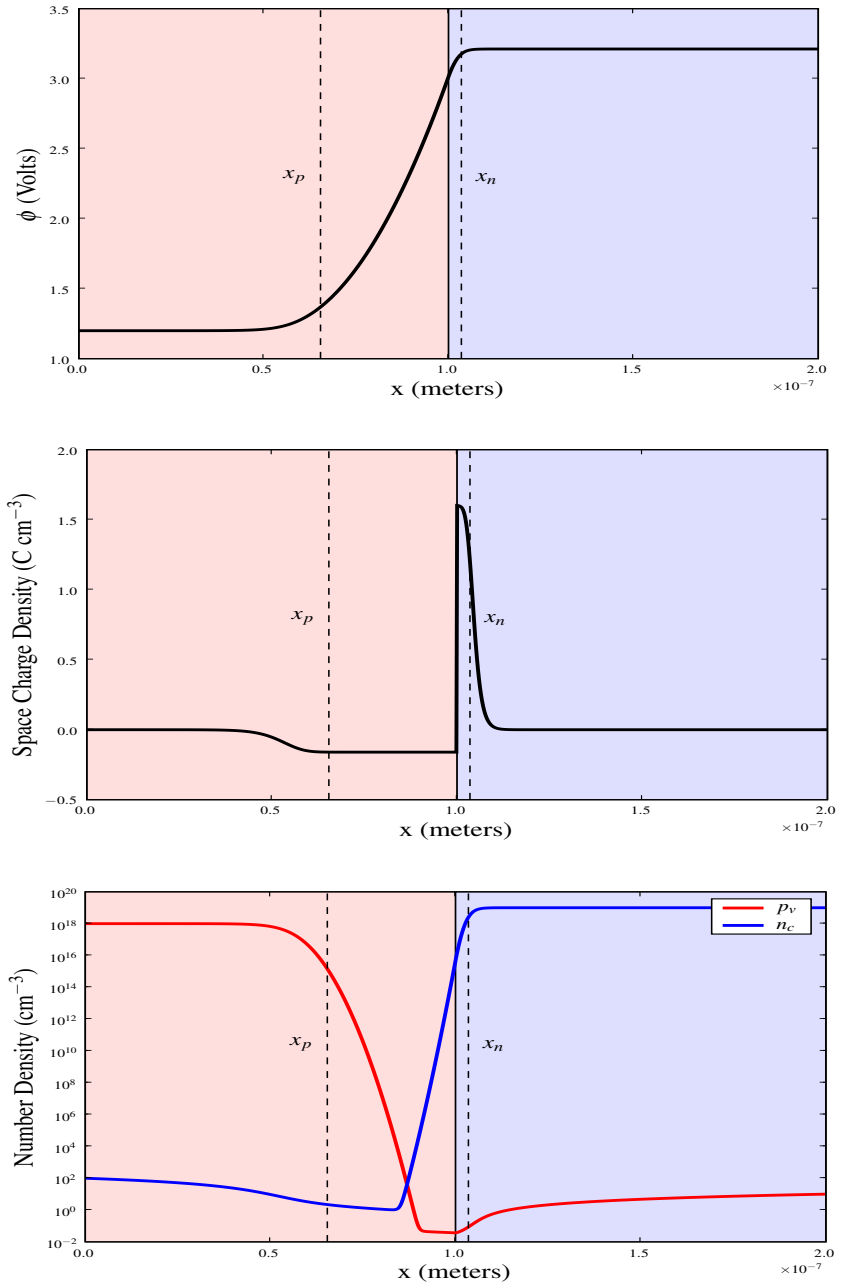

Figure C.3: Potential (ϕ), charge density, and number density of holes and electrons for the numerical simulation of an abrupt PN junction under reverse bias with $V_{bias} = 1.2$ V. The depletion region boundaries x_p and x_n shown are the ones calculated for the case where $V_{bias} = 0$ V to illustrate the increase in the width of the depletion region.

The same methodology used here will be applied to the PIN diodes in the HyViSI detectors. With the proper grid spacing and time step-size, we should expect that valid results will be obtained for structures more complex than the simple PN junction.

C.5 Cylindrically Symmetric Persistence Simulations

Two or three dimensional finite difference numerical simulations are difficult to carry out. This is especially true when an implicit method is used, as the two or three dimensions must be handled with different techniques. For radially symmetric phenomena, such as persistence in hybrid detectors, using polar coordinates reduces the complexity of the difference scheme, saves computation time and memory, and may potentially increase numerical stability.

We begin by considering cylindrically symmetric distributions of electrons, n, and holes, p, whose dynamics are governed by the semiconductor Equations C.1-C.7. In the context of the actual detector layer, these distributions would obviously have some extent in the z direction, but we ignore this and collapse them into a plane at $z = 0$, which corresponds to the front side of the detector. We will assume that excess carriers can still be lost to diffusion and subsequent recombination in the z direction, but after these particles have left the plane they will no longer be tracked. We will further make the simplifying assumption that the equilibrium carrier concentrations, p_v^o and n_v^o, balance the ionized donors, N_d^+ and N_a^-, so that these four species make no net contribution to the charge density, and thus no contribution to the radial electric field. The only contribution to the charge density and radial electric field then arises purely from the excess of carriers n and p. We will denote the number of electrons at radius r and time t as $n(r,t)$ and the number of holes as $p(r,t)$.

We will assume that the electrons are free to move in the radial direction and that generation is negligible, i.e. $G_n = 0$. The continuity equation governing the electron distribution can then be written as:

$$\frac{\partial n}{\partial t} = \nabla \cdot (\mathbf{J}_{Diff} + \mathbf{J}_{Drft}) - U_n = \frac{2J_{Diff}}{r} + \frac{\partial J_{Diff}}{\partial r} + \frac{2J_{Drft}}{r} + \frac{\partial J_{Drft}}{\partial r} - U_n, \tag{C.24}$$

where J_{Diff} is the electron diffusion current given by

$$J_{Diff} = D_n \nabla n(r,t) = D_n \frac{\partial n}{\partial r}\hat{r}, \tag{C.25}$$

J_{Drft} is the electron drift current given by

$$J_{Drft} = \mu_n n E_r \hat{r}, \tag{C.26}$$

and U_n is the rate of recombination, which will be considered shortly. D_n is the diffusion coefficient with units of $[length^2][time^{-1}]$, μ_n is the mobility with units of $[length^2][V^{-1}][time^{-1}]$, and E_r is

the radial electric field. Note that the currents are in terms of particles per unit time and not charge per unit time.

For reasons discussed in the text, the hole distribution is assumed to consist of immobile holes and contain no source of generation when the detector is not illuminated, i.e. $G_p = 0$.[1] It only changes through recombination with electrons,

$$\frac{\partial p}{\partial t} = -U_p = -\frac{pn}{\tau_p(n+p)}. \tag{C.27}$$

Under the assumption that the traps responsible for recombination are deep level traps, this recombination requires that an electron be removed from the conduction band as well, which means $U_n = U_p$. The trapped holes may very well exist outside of the plane $z = 0$, meaning the electrons lost through U_n need to drift or diffuse in the z direction to reach the recombination sites, and a true 2d simulation would need to account for this. Since transport of the electrons to the recombination sites is neglected, the simulation is only quasi-2d.

Substituting Equations C.25 and C.27 into C.24 yields the form that will be used to be solved for the electron distribution evolution. Along with the hole distribution equation and Gauss's Law for the electric field, the governing equations then have the form:

$$\frac{\partial n}{\partial t} = D_n\left(\frac{2}{r}\frac{\partial n}{\partial r} + \frac{\partial^2 n}{\partial r^2}\right) + \frac{2J_{Drft}}{r} + \frac{\partial J_{Drft}}{\partial r} - \frac{pn}{\tau_p(p+n)} \tag{C.28}$$

$$\frac{\partial p}{\partial t} = -\frac{pn}{\tau_p(n+p)} \tag{C.29}$$

$$\frac{\partial E_r}{\partial r} = \frac{p-n}{\epsilon} - \frac{2}{r}E_r \tag{C.30}$$

These are the equations that will be used to evolve the particle distributions in time.

Since the governing equation involves only one spatial dimension, a regularly, finely spaced grid of radial points r_i (from $r = r_o$ to $r = r_{max}$) can be used without creating memory allocation problems or significantly slowing the evolution of the system. This means all $\Delta r = r_{i+1} - r_i$ are equal in the grid. With second order centered difference schemes for the first and second spatial derivatives and a first order explicit time derivative, Equations C.29 and C.28 become

$$\frac{n_i^{k+1} - n_i^k}{\Delta t} = D_n\left(\frac{2}{r_i}\frac{n_{i+1}^k - n_{i-1}^k}{2\Delta r} + \frac{n_{i+1}^k - 2n_i^k + n_{i-1}^k}{\Delta r^2}\right) + \frac{2J_i^k}{r_i} + \frac{J_{i+1}^k - J_{i-1}^k}{2\Delta r} - \frac{p_i n_i}{\tau_p(n_i + p_i)} \tag{C.31}$$

$$\frac{p_i^{k+1} - p_i^k}{\Delta t} = -\frac{p_i n_i}{\tau_p(p_i + n_i)} \tag{C.32}$$

[1] A constant term G_p can be included to extend to the case where the detector is illuminated with a weak background flux. The results do not change significantly, so G_p is kept at zero here.

where k is the time index that relates the time elapsed t to the time increment Δt via $t = k\Delta t$. $J_i^k = J_{Drft}$ is the electron drift current at $r = r_i$ and time-step k given by

$$J_i^k = \mu_n n_i^k E_i^k. \tag{C.33}$$

Since Equation C.31 requires the electric field at each grid point be known, at each time-step, the electric field is first solved for using a backward difference scheme:

$$E_{i-1} = \Delta r \left(-\frac{2}{r_i} E_i + \frac{1}{\Delta r} E_i + \frac{p_i - n_i}{\epsilon} \right). \tag{C.34}$$

Starting at the maximum radius in the grid, $r = r_{max}$, far away from the electron and hole distributions so that $p = n = 0$ and $E = 0$, we integrate this toward $r = 0$ to obtain the electric field. Because the field would diverge at the origin, E_o is not included in the calculation, and instead set to zero. At each time-step k, Equation C.34 is used to solve for the field and then C.31 and C.32 are used to advance the solution forward in time.

The boundary condition for the electron distribution at the origin r_o is easily handled by recognizing that the first derivative is necessarily zero and then using the radial symmetry to create an imaginary point $r_{-1} = r_1$ that can be used for the second derivative:

$$n_0^{k+1} = n_0^k + D_n \Delta t \left(\frac{2n_1^k - 2n_0^k}{\Delta r^2} \right) - \frac{p_o}{\tau_p}. \tag{C.35}$$

And to reiterate, if r_{max} is made sufficiently large then the particles and field will not reach the other boundary, so $n_{i_{max}}^{k+1} = n_{i_{max}}^k = 0$, and so on for the other variables. With the computational method in place, the only thing that remains is to specify the initial distributions $n(r, 0)$ and $p(r, 0)$.

In choosing a set of units for the simulation, it turns out to be easiest to treat r in terms of pixels. This is because small numbers like the pixel pitch of 18×10^{-6} m necessitate very small time steps and contribute significantly to roundoff error in the divisions and multiplications used in the calculation, and this in turn decreases numerical stability. After the calculation is finished, the results can be easily converted to physically meaningful quantities via the following equations:

$$D_n^{phys} = D_n^{sim} * p^2 \tag{C.36}$$

$$\mu_n^{phys} = \mu_n^{sim} * p^2, \tag{C.37}$$

where p is the pixel pitch in cm.